Reactions of Pt^+ with H_2, D_2, and HD: Effect of lanthanide contraction on reactivity and thermochemistry

Xiao-Guang Zhang and P. B. Armentrout
Department of Chemistry, University of Utah, Salt Lake City, Utah 84112-0850

(Received 16 November 2001; accepted 9 January 2002)

A guided ion beam tandem mass spectrometer is used to examine the kinetic energy dependence of reactions of the third-row transition metal cation, Pt^+, with molecular hydrogen and its isotopologs. A flow tube ion source produces Pt^+ ions in its electronic ground state term and primarily in the lowest spin–orbit level. Corresponding state-specific reaction cross sections are obtained. Modeling of the endothermic reaction cross sections yields the 0 K bond dissociation energy of $D_0(Pt^+-H)=2.81\pm0.05$ eV (271 ± 5 kJ/mol). The experimental thermochemistry is consistent with *ab initio* calculations, performed here and in the literature. Theory also provides the electronic structures of these species and is used to examine the reactive potential energy surfaces. Results from reactions with HD provide insight into the reaction mechanisms and indicate that the late metal ion, Pt^+, reacts largely via a direct mechanism. Results for this third-row transition metal system are compared with the first-row and second-row congeners and found to have higher reactivity towards dihydrogen and stronger M^+-H bonds. These differences can be attributed to lanthanide contraction and relativistic effects. © *2002 American Institute of Physics.* [DOI: 10.1063/1.1456028]

I. INTRODUCTION

There are numerous experimental studies of the reactions of the ions of atomic first-row transition metals,[1–10] second-row transition metals,[9–13] third-row transition metals,[11] and other metals[14–18] with dihydrogen, reaction (1), and its isotopic analogs,

$$M^+ + H_2 \rightarrow MH^+ + H. \quad (1)$$

Such studies provide insight into the electronic requirements for the activation of dihydrogen by single metal centers and periodic trends in the reactivity of metal ions.[4,7,9–13,19,20] Although simple, this reaction allows a detailed study of the activation of a covalent single bond, directly analogous to the activation of the C–H and C–C bonds of hydrocarbons in homogeneous and heterogeneous catalytic processes.[21,22] The guided ion beam methods used in our laboratory have the particular strength that bond dissociation energies (BDEs) for M^+-H can be derived from the kinetic energy dependence of reaction (1).[23–25] The thermochemistry obtained from these studies is of obvious fundamental interest and also has implications for understanding a variety of catalytic reactions involving transition metal systems.[21,22] Further, these relatively small systems form an ideal interface between experiment and theory.

Compared to the first and second rows, experimental gas-phase studies are less extensive for third-row transition-metal cations, as only La^+ and Lu^+ have been studied.[11] However, theoretical studies include all of the third-row transition-metal cations.[26–33] To augment the existing experimental data for such systems, an ongoing project in our laboratory is to use guided ion beam tandem mass spectrometry to systematically study the activation of H_2 by third-row transition metal cations and determine the M^+-H BDEs. In this work, we report absolute cross sections as a function of kinetic energy for reactions of dihydrogen with Pt^+ and analyze them to acquire $D_0(Pt^+-H)$. To assign electronic structures and explore possible mechanisms, theoretical calculations on the PtH^+ and PtH_2^+ species were also performed. Although our experiments with H_2 and D_2 allow a determination of bond energies and reactivities, these systems supply little information about the reaction mechanisms. Therefore, we also investigate the reactions of Pt^+ with HD over a wide range of kinetic energies. Such reactions with HD have previously been shown to provide useful mechanistic information.[7,9,11–13,19,20] Finally, we compare the reactivities and mechanisms of this transition metal ion with those of its congeners in the first and second transition metal series.[7,12]

II. EXPERIMENT

A. General procedures

The guided ion beam tandem mass spectrometer on which these experiments were performed has been described in detail previously.[34,35] Briefly, atomic metal ions are generated in a direct current discharge flow tube source described below, extracted from the source, accelerated, and focused into a magnetic sector momentum analyzer for mass selection of primary ions. The mass-selected ions are decelerated to a desired kinetic energy and focused into an octopole ion beam guide that uses radio-frequency electric fields to trap the ions in the radial direction and ensure complete collection of reactant and product ions.[36,37] The octopole passes through a static gas cell with an effective length of 8.26 cm that contains the reaction partner at a low pressure (usually $\lesssim$0.3 mTorr) so that multiple ion–molecule collisions are improbable. All products reported here result from single bimolecular encounters, as verified by pressure dependence studies. The unreacted parent and product ions are

confined radially in the guide until they drift to the end of the octopole where they are extracted, focused, and passed through a quadrupole mass filter for mass analysis of products. Ions are subsequently detected with a secondary electron scintillation ion detector using standard pulse counting techniques. Reaction cross sections are calculated from product ion intensities relative to reactant ion intensities after correcting for background signals.[38] Uncertainties in absolute cross sections are estimated to be ±20%.

The kinetic energy of the ions is varied in the laboratory frame by scanning the dc bias on the octopole rods with respect to the potential of the ion source region. Laboratory (lab) ion energies are converted to energies in the center-of-mass frame (CM) by using the formula $E_{CM}=E_{lab}m/(m+M)$, where m and M are the neutral and ionic reactant masses, respectively. Two effects broaden the cross section data: the kinetic energy distribution of the reactant ion and the thermal motion of the neutral reactant gas (Doppler broadening).[39] The absolute zero and the full width at half maximum (FWHM) of the kinetic energy distribution of the reactant ions are determined using the octopole beam guide as a retarding potential analyzer, as described previously.[38] The distributions of ion energies, which are independent of energy, are nearly Gaussian and have a typical FWHM of 0.3–0.6 eV (lab) in these studies. Uncertainties in the absolute energy scale are ±0.05 eV (lab).

B. Ion source

Atomic metal ions are produced in a direct current discharge flow tube (DC/FT) source,[35] consisting of a cathode held at high negative voltage (0.7–1.5 kV) over which a flow of approximately 90% He and 10% Ar passes at a total pressure of 0.3–0.5 Torr and ambient temperature. In this work, the cathode is platinum foil attached to an iron holder. Ar^+ ions created in the discharge are accelerated toward the metal cathode, thereby sputtering Pt^+ ions, which are then swept down a 1 m long flow tube. The ions undergo ~10^5 thermalizing collisions with He and ~10^4 collisions with Ar before entering the guided ion beam apparatus. Generally, these conditions are sufficient to produce atomic ions in their ground electronic state. However, trace amounts of low-lying excited states of Pt^+ are observed to survive these flow conditions, as found by examining the test reaction of Pt^+ with O_2.[40] These excited species are easily removed by introducing O_2 to the flow tube about 15 cm downstream of the discharge zone at a pressure of ~150 mTorr.

With the addition of this cooling gas, the DC/FT source produces metal ions in the ground state. For example, on the basis of comparisons to a surface ionization source, the DC/FT source was found to generate Sc^+,[41] Fe^+,[42] Co^+,[43] Ni^+,[44] Ru^+,[12] Rh^+,[12] and Pd^+ (Ref. 12) ions with an average electronic temperature of 700±400 K, and Y^+, Zr^+, Nb^+, and Mo^+ ions with an average electronic temperature of 300±100 K.[13] Therefore, M^+ ions created under such conditions are believed to be in the ground electronic state term, $a\,^2D(5d^9)$ for Pt^+,[45] and largely in the lowest spin–orbit level (Table I). From the populations of ions at 700 ±400 K, the average electronic energy is calculated to be ≤0.002 eV for Pt^+. These estimated populations are consistent with the failure to observe any evidence for electronically excited Pt^+ species in the present and related studies,[40,46] once the cooling gases are added to the flow tube.

TABLE I. Electronic states of platinum cations.[a]

State	J	Electron configuration	Energy (eV)	Population (%)[b] 300 K	700 K	1100 K
^2D	5/2	$5d^9$	0.000	100.00	99.99	99.68
^4F	9/2	$6s^15d^8$	0.593	0.0	0.01	0.32
^2D	3/2	$5d^9$	1.044	0.0	0.0	0.0
^4F	7/2	$6s^15d^8$	1.160	0.0	0.0	0.0

[a]Reference 45.
[b]Maxwell–Boltzmann distribution at the indicated temperature.

C. Data analysis

The kinetic-energy dependence of product cross sections is analyzed to determine E_0, the energy threshold for product formation at 0 K. E_0 differs from the apparent threshold observed under laboratory conditions because of the Maxwell–Boltzmann velocity distribution and internal energy of the neutral reactants, and the kinetic distribution of the reactant ions. Each of these contributions allows reactions to occur at energies below E_0. To determine E_0, endothermic reaction cross sections are modeled using Eq. (2),[23–25,47–50]

$$\sigma(E)=\sigma_0\Sigma g_i(E+E_{el}+E_i-E_0)^n/E, \quad (2)$$

where σ_0 is an energy-independent scaling factor, E is the relative kinetic energy of the reactants, E_{el} is the electronic energy of the metal cation, and n is an adjustable parameter. The sum considers contributions from rovibrational states of the neutral reactants at 300 K, denoted by i, having energies E_i and populations g_i, where $\Sigma g_i=1$. As noted above, E_{el} at 700±400 K is believed to be ≤0.002 eV for Pt^+. The various sets of vibrational frequencies and rotational constants used to determine E_i in this work are taken from the literature for H_2, D_2, and HD.[51] Before comparison with the experimental data, Eq. (2) is convoluted with the kinetic energy distributions of the atomic ions and neutral reactants at 300 K. The σ_0, n, and E_0 parameters are then optimized using a nonlinear least-squares analysis to give the best reproduction of the data.[38] Error limits for E_0 are calculated from the range of threshold values for different data sets over a range of acceptable n values combined with the absolute errors in the kinetic energy scale and electronic energies.

III. THEORETICAL CALCULATION

All quantum chemistry calculations reported here are computed using the B3LYP hybrid density functional method,[52,53] and performed with the GAUSSIAN 98 suite of programs.[54] A large basis set is used for hydrogen, triple zeta with diffuse and polarization functions, 6-311+G(3p). This basis set gives good results for the thermochemistry of dihydrogen, with deviations from experiment of less than 0.03 eV for the bond energy of H–H (4.505 eV calculated versus 4.478eV experimental[51]). The 60 core electrons of platinum

TABLE II. Calculated vibrational frequencies and zero point energies.[a]

Species	Frequencies (cm^{-1})	Zero point energy (eV)
H_2	4331	0.268
$Pt^+-H(^1\Sigma^+)$	2403	0.149
$(^3\Delta)$	2275	0.141
$Pt^+-H_2(^2A_1)$[b]	787, 2333, 2361	0.340
$(^2A_2)$[b]	642, 2115, 2255	0.311
$(^2A_2)$[c]	930, 1705, 2428	0.314
$(^2B_1)$[b]	836, 2253, 2280[d]	0.333
$(^2B_1)$[c]	732, 1320, 2854	0.304
$(^2B_2)$[c]	606, 653, 3753	0.311

[a]Calculations using B3LYP/6−311+G(3p) on H and Hay–Wadt relativistic ECP (Ref. 55) as adjusted for the metal cation by Ohanessian *et al.* (Ref. 26). All frequencies have been scaled by 0.9804.
[b]These species have H–Pt^+–H structures.
[c]These species have $Pt^+-(H_2)$ structures.
[d]The asymmetric stretch is calculated as being imaginary, but relaxation of C_{2v} symmetry collapses this state to the $^2A_1$ ground state. This frequency is assigned from the symmetric stretch using the same ratio as these frequencies for the $^2A_1$ state.

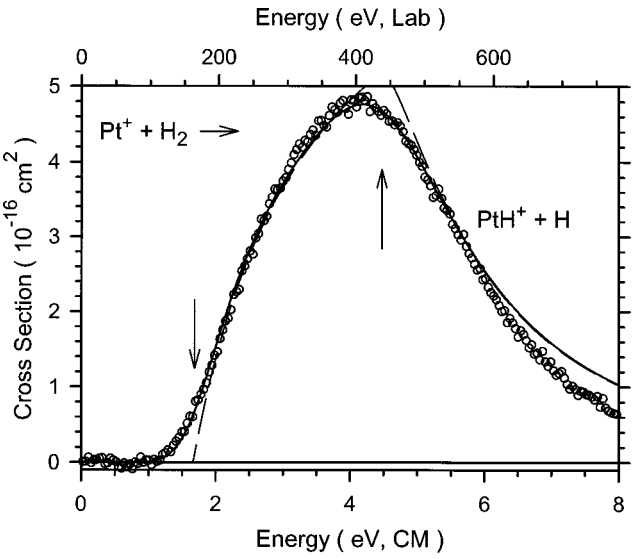

FIG. 1. Cross sections for reaction of Pt^+ (^2D) with H_2 as a function of kinetic energy in the center-of-mass frame (lower axis) and laboratory frame (upper axis). The best fit of Eq. (2) with parameters of Table II to the data is shown as a dashed line. The solid line shows this model convoluted over the kinetic and internal energy distributions of the reactant neutral and ion. The arrows indicate E_0 and D_0(H–H) at 4.478 eV.

are described by the relativistic effective core potentials (ECPs) of Hay-Wadt (HW),[55] equivalent to the Los Alamos double zeta ECP (LANL2DZ) basis set. The HW-ECP is optimized for neutral atoms, whereas the positive charge differentially contracts the s orbitals compared to the d orbitals. Hence, calculations were performed with an altered HW-ECP basis for Pt^+ as described by Ohanessian *et al.* (HW+).[26] We previously have reported results on PtH^+ for both the HW and HW+ basis sets,[46] and also performed single point energy calculations, using the HW+-ECP geometries, in which the HW-ECP was expanded as described by Pavlov *et al.* (by uncontracting one s, one p, and one d function and adding one diffuse d function and two f functions)[56] and we contracted the s orbitals as described by Ohanessian *et al.* (HW+X).[26,46] In all cases, the thermochemistry calculated here is corrected for zero point energy effects, which were explicitly calculated for each state of H_2, PtH^+, and PtH_2^+. The calculated frequencies, scaled by 0.9804,[57] are listed in Table II.

The experimental BDE refers to the ground spin–orbit state at 0.0 eV, $a\ ^2D_{5/2}$ for Pt^+.[45] In contrast, calculations are referenced to the properly weighted mean of all spin–orbit levels in the ground state term, 0.418 eV for $Pt^+(a\ ^2D)$.[45,46,56] Because our calculations do not explicitly include spin–orbit interactions, all calculated bond energies must be corrected by these different asymptotic energies to properly compare with experimental values. This correction improves the agreement between experiment and the theory conducted here, a result also obtained in the following paper[58] and in our work on $PtCH_x^+$ species.[46] Likewise the description of the generalized valence bond (GVB) calculations of Ohanessian *et al.*[26] and the CASSCF and MRSDCI calculations of Zhang and Balasubramanian[33] suggest that such corrections may also need to be applied to their reported bond energies in order to properly compare with our experimental results. (Although it is possible that such corrections have already been made.) As will be seen below, however, the literature values as reported agree so much better with our experimental values that we do not apply such a correction to their values in the results and discussion below.

IV. EXPERIMENTAL RESULTS

A. Reactions with H_2 and D_2

Figure 1 shows cross sections as a function of kinetic energy for the bimolecular reaction of H_2 with Pt^+ produced in the DC/FT source. A single product ion, as shown in reaction (1), is observed. Comparable results for reaction with D_2, process (3), are shown in Fig. 2,

$$Pt^+ + D_2 \rightarrow PtD^+ + D. \tag{3}$$

The magnitudes of the $Pt^+ + H_2$ and $Pt^+ + D_2$ reaction cross sections are well within the 20% experimental uncertainty of these absolute cross section measurements when the same mass resolution for the quadrupole mass spectrometer is used. Results of the reaction $Pt^+ + D_2$ are easier to acquire because the heavier isotope reduces mass overlap between the product ion and the much more intensive primary ion, thereby allowing intensities of the product ion to be measured more accurately over a larger dynamic range.

The cross sections rise from an apparent threshold and reach maxima near the dissociation energy of H_2, 4.478 eV, or D_2, 4.56 eV.[51] Above this energy, PtH^+ (PtD^+) may be formed with an internal energy in excess of its bond dissociation energy. Thus, the PtH^+ (PtD^+) product begins to dissociate in the overall reaction (4),

$$Pt^+ + H_2(D_2) \rightarrow PtH^+(PtD^+) + H(D) \rightarrow Pt^+ + 2H(D). \tag{4}$$

The experimental cross sections reach maxima slightly below the H_2 (D_2) bond energy. This is a result of the broadening induced by the kinetic energy distributions, as shown

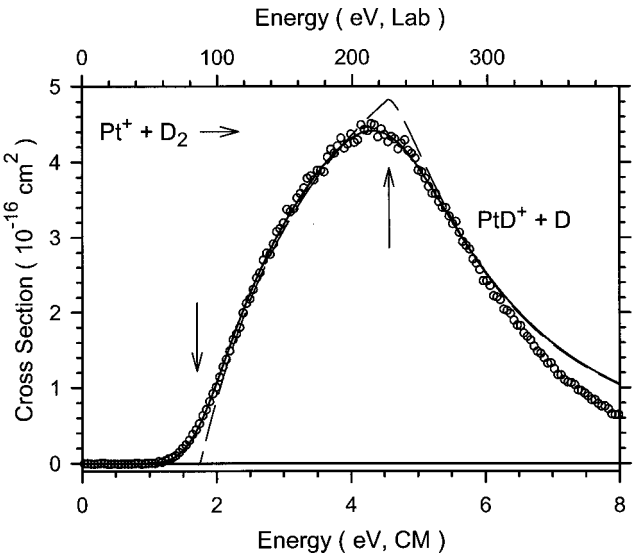

FIG. 2. Cross sections for reaction of Pt^+ (^2D) with D_2 as a function of kinetic energy in the center-of-mass frame (lower axis) and laboratory frame (upper axis). The best fit of Eq. (2) with parameters of Table II to the data is shown as a dashed line. The solid line shows this model convoluted over the kinetic and internal energy distributions of the reactant neutral and ion. The arrows indicate E_0 and D_0(D–D) at 4.56 eV.

by the good agreement between the data and our modeling with the onset for reaction (4) fixed to the appropriate thermodynamic value, discussed further below.

B. Reactions with HD

Pt^+ reacts with HD to yield both processes (5) and (6), as shown in Fig. 3,

$$Pt^+ + D_2 \rightarrow PtH^+ + D \quad (5)$$

$$\rightarrow PtD^+ + H. \quad (6)$$

Because of the close proximity of the product masses, there is some overlap between these signals at the mass resolution

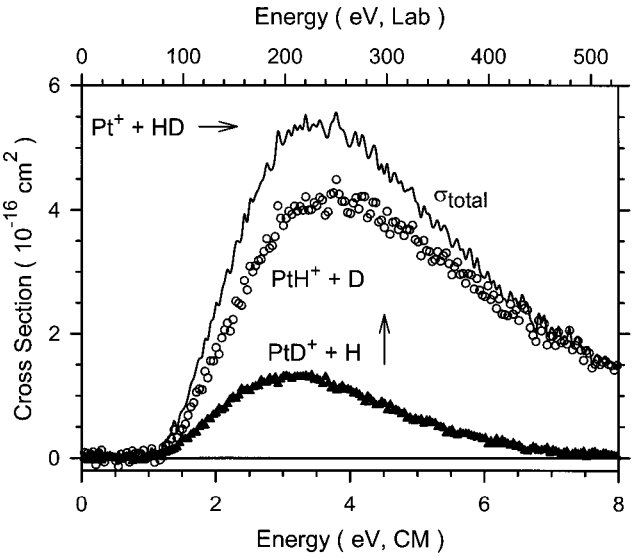

FIG. 3. Cross sections for reaction of Pt^+ (^2D) with HD as a function of kinetic energy in the center-of-mass frame (lower axis) and laboratory frame (upper axis). The arrow indicates D_0(H–D) at 4.51 eV.

TABLE III. Parameters of Eq. (2) used in modeling reactions (1) and (3) and the resultant bond energies.

Reaction	σ_0	n	E_0 (eV)	$D_0(Pt^+–H)$ (eV)
$Pt^+ + D_2$	7.5±0.4	1.1±0.1	1.71±0.05	2.81±0.05[a]
$Pt^+ + H_2$	7.4±0.5	1.1±0.1	1.68±0.06	2.80±0.06

[a]Value corrected for the zero-point energy difference. See text.

used in the quadrupole mass filter. Resolution could not be increased further without sacrificing efficient collection of the product ions. This mass overlap has been carefully measured by determining peak shapes with and without gas in the collision cell. Although the similar energy dependence of the two products makes such measurements somewhat difficult, the mass overlap contribution of the higher mass PtD^+ channel to the PtH^+ channel has been subtracted in the cross sections shown. The accuracy of this correction is confirmed by good agreement between the magnitudes of the total cross sections for the HD system and those of the H_2 and D_2 systems (Figs. 1 and 2).

Both PtH^+ and PtD^+ cross sections exhibit endothermic behavior and rise from thresholds that are similar to each other and to those of the H_2 and D_2 systems. The cross sections of PtH^+ and PtD^+ peak slightly below the bond dissociation energy of HD, 4.51 eV,[51] with those for PtD^+ peaking at somewhat lower energies than those of PtH^+. The total cross section in the HD system is similar in shape to the D_2 and H_2 data at energies below the maximum cross section, whereas at higher energies, the total cross section, largely attributable to the $PtH^+ + D$ channel, exceeds those of the D_2 and H_2 systems. Such a result indicates that the PtH^+ product ion is stabilized by removal of energy by the D atom product. The relative high-energy behavior shows that the D atom carries away more energy from PtH^+ than the H atom carries away from PtD^+, and more than the neutral products carry away in the H_2 and D_2 systems, as well. This interesting effect is typical of atomic ion reactions with H_2, HD, and D_2,[9,12,13,20] and has been discussed in detail elsewhere.[20,59–61]

V. THERMOCHEMICAL AND THEORETICAL RESULTS

A. Thermochemistry

The endothermic cross sections in the H_2 and D_2 reaction systems are analyzed in detail using Eq. (2). Typical models are shown in Figs. 1 and 2 and can be seen to reproduce the experimental results very well. At energies above the onset of reaction (4), our analyses include a model for this subsequent dissociation, as outlined in detail elsewhere.[62] This model relies on two parameters, E_D, the onset for PtH^+ (PtD^+) dissociation in reaction (4), and p, a parameter similar to n in Eq. (2). For the results shown in Figs. 1 and 2, E_D is fixed to the H_2 (D_2) bond energy and the optimum value of p was found to be 2.0.

The optimum values of the parameters in Eq. (2) are listed for these systems in Table III. These values represent

the average of between 5–9 data sets for each system. Note that the thresholds listed differ appreciably from the apparent thresholds for these reactions as shown in Figs. 1 and 2. This is largely because of the appreciable kinetic energy distribution of the light H_2 or D_2 reactant. Because the rotational, vibrational, translational, and electronic energy distributions of reactants are explicitly included in the modeling, the E_0 threshold energies determined using Eq. (2) correspond to 0 K values. From the thresholds measured, the BDEs for the metal–ligand cations observed in the reactions (1) and (3) can be calculated using Eq. (7),

$$D_0(Pt^+-L)=D_0(L-L)-E_0, \tag{7}$$

where $D_0(H-H)=4.478$ eV and $D_0(D-D)=4.556$ eV.[51] This equation assumes that there is no activation barrier in excess of the endothermicity of the reaction, an assumption that is often true for ion-molecule reactions because of the long-range attractive forces.[49] Table III provides a summary of the Pt^+-H bond energies derived from the present experiments with both H_2 and D_2. For the D_2 results, this requires correcting for the zero point energy differences between PtD^+ and PtH^+. This correction uses a vibrational frequency of 2399 cm^{-1} for PtH^+,[26] in excellent agreement with our calculated value of 2403 cm^{-1} for the $^1\Sigma^+$ state (Table II). The vibrational frequency of PtD^+ is calculated from that of PtH^+ according to $\omega_{PtD}=\omega_{PtH}(\mu_{PtH}/\mu_{PtD})^{1/2}$. Thus the zero point energy differences in the PtH^+ and PtD^+ bond energies are 0.043 ± 0.004 eV, assuming a 10% uncertainty in the frequency. (Use of the 2275 cm^{-1} frequency calculated here for the $^3\Delta$ state, Table II, yields a difference of 0.041 eV, which does not change the final results.) Note that the Pt^+-H bond energies obtained from the H_2 and D_2 systems are in excellent agreement with one another (Table III). We take the average of these two values as our final experimental determination of 2.81 ± 0.05 eV (271 ± 5 kJ/mol).

B. PtH^+ electronic structure

GVB calculations indicate that the Pt^+-H bond in the $^1\Sigma^+$ state is formed by covalent interaction between the singly occupied $5d\sigma$ orbital on Pt^+ (89% $5d$ and 11% $6s$) and the singly occupied $1s$ orbital on H.[26] This bonding scheme requires no promotion from the ground electronic state of $Pt^+(^2D,5d^9)$ and no loss of exchange energy, which seems consistent with a strong bond. The calculations also indicate that there is a low-lying $^3\Delta$ state formed from interaction of $Pt^+(^4F,6s^15d^8)$ with $H(^2S,1s)$.[26] Here, the bonding orbital on Pt is a $6s-5d\sigma$ hybrid, which for the rest of the third row metal ions involves approximately a 60% $5d$ and 40% $6s$ combination of orbitals.[26] Interestingly, even though binding to $Pt^+(^4F,6s^15d^8)$ requires both promotion and the loss of exchange energy, the $6s-5d\sigma$ hybrid bonding orbital overlaps better with the $1s$ orbital of H, such that GVB calculations find that the $^3\Delta$ state lies only 0.04 eV above the $^1\Sigma^+$ state.[26] Spin–orbit interactions are suggested to invert the order of these states.

Our calculations using the HW, HW+, and HW+X ECPs find that the $^3\Delta$ is the ground state by 0.19, 0.10, and 0.14 eV, respectively. The bond energies for this state (corrected for the spin-orbit state splitting of the Pt^+ asymptote), 2.79, 2.65, and 2.70 eV, respectively, are close to the experimental value of 2.81 ± 0.05 eV (Table IV). Likewise, GVB theory followed by correlation consistent configuration interaction (CCCI) calculations[26] provides BDEs of 2.69 eV for the $^3\Delta$ state and 2.73 eV for the $^1\Sigma^+$ state, also in reasonable agreement with experiment. (Note that a correction for the Pt^+ spin–orbit asymptote would decrease the GVB values by 0.418 eV, making them disagree considerably with experiment and the present calculations.) For both states, the bond lengths calculated here agree reasonably well with those from Ohanessian *et al.* (Table V). Overall, it seems likely that the $^3\Delta$ state is the true ground state for PtH^+.

TABLE IV. Comparison of experimental and theoretical bond energies (in eV) for PtH^+ and PtH_2^+.

Species	Experiment	Theory	
		This work[a]	Literature[b]
$Pt^+-H(^1\Sigma^+)$	2.81 ± 0.05	2.55	2.73[c]
$(^3\Delta)$		2.65	2.69[c]
$Pt^+-H_2(^2A_1)$[d]	1.52 ± 0.12[e]	1.60	1.20 (0.59)[f]
$(^2A_1)$[g]		*U*	0.72 (0.32)[f]
$(^2A_2)$[d]		0.91	*U*
$(^2A_2)$[g]		0.91	0.69 (0.30)[f]
$(^2B_1)$[d]		0.72	0.04 (−0.52)[f]
$(^2B_1)$[g]		0.25	0.28 (0.12)[f]
$(^2B_2)$[g]		−0.06	0.23 (0.13)[f]

[a]Calculations using B3LYP/6−311+G(3*p*) on H and the Hay–Wadt relativistic ECP (Ref. 55) as adjusted for the metal cation by Ohanessian *et al.* (Ref. 26). All values corrected for zero point energies and for the spin–orbit state splitting of the Pt^+ asymptote.
[b]Values may need to be adjusted to correct for the spin–orbit splitting of the Pt^+ asymptote. See text.
[c]Ohanessian *et al.* (Ref. 26).
[d]These species have $H-Pt^+-H$ structures. *U* indicates the structure collapses to the $Pt^+-(H_2)$ structure at this level of theory.
[e]Zhang, Liyanage, and Armentrout (Ref. 46).
[f]Zhang and Balasubramanian (Ref. 33). MRSDCI (CASSCF) values.
[g]These species have $Pt^+-(H_2)$ structures. *U* indicates the structure collapses to the $H-Pt^+-H$ structure at this level of theory.

TABLE V. Theoretical geometries for PtH^+ and PtH_2^+.

Species	This work[a]		Literature[b]	
	r_e (Pt–H, Å)	∠HPtH (°)	r_e (Pt–H, Å)	∠HPtH (°)
$Pt^+-H(^1\Sigma^+)$	1.518		1.519[c]	
$(^3\Delta)$	1.544		1.531[c]	
$PtH_2^+(^2A_1)$	1.530	83.3	1.53	81.1
$(^2A_1)$[d]	*U*	*U*	1.73	29.6
$(^2A_2)$[d]	1.554	67.8	*U*	*U*
$(^2A_2)$	1.678	32.1	1.88	25.5
$(^2B_1)$	1.557	91.6	1.56	89.7
$(^2B_1)$	1.818	27.4	2.12	20.9
$(^2B_2)$	2.059	22.0	2.32	19.0

[a]Calculations using B3LYP/6−311+G(3*p*) on H and the Hay–Wadt relativistic ECP (Ref. 55) as adjusted for the metal cation by Ohanessian *et al.* (Ref. 26).
[b]Except as noted, MRSCDI values from Zhang and Balasubramanian (Ref. 33).
[c]GVB/CCCI results from Ohanessian *et al.* (Ref. 26).
[d]*U* indicates the structure collapses to the other type of structure at this level of theory.

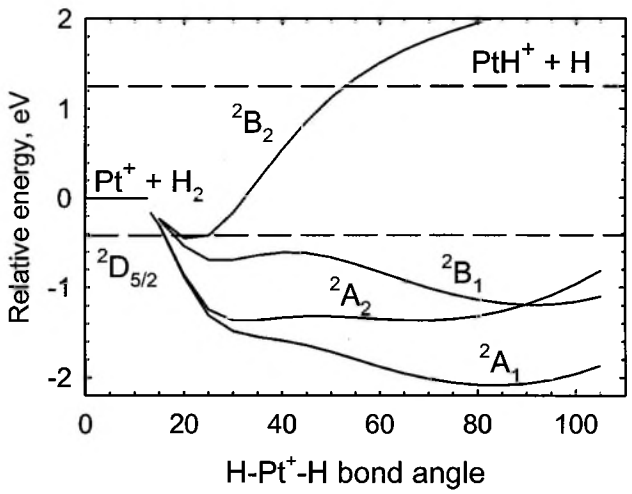

FIG. 4. B3LYP/HW+/6-311+G(3p) calculations of the potential energy surfaces for the interaction of $Pt^+(^2D)$ with H_2 in C_{2v} symmetry as a function of the H–Pt^+–H bond angle in degrees. Dashed lines indicate the experimental energy zero, corresponding to the $Pt^+(^2D_{5/2})$ ground state at −0.418 eV, and the experimental energy of the PtH^+ + H products, 1.67 eV above the experimental $Pt^+(^2D_{5/2})+H_2$ ground state asymptote.

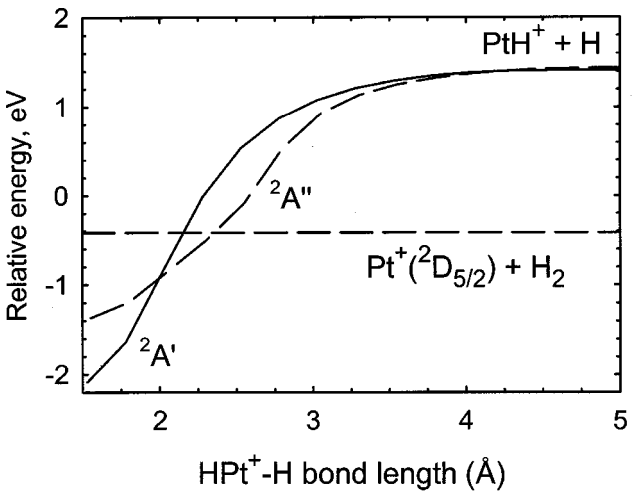

FIG. 5. B3LYP/HW+/6-311+G(3p) calculations of the potential energy surfaces for the dissociation of $PtH_2^+(^2A',^2A'')$ to form PtH^+ + H as a function of the HPt^+–H bond length in angstroms. A dashed line indicates the experimental energy zero, corresponding to the $Pt^+(^2D_{5/2})$ ground state at −0.418 eV.

C. $Pt^+ + H_2$ reaction surfaces

To explore coarse features of the potential energy surface for reaction (1), we also calculated the properties of stable PtH_2^+ complexes. Our results can be compared directly with those of Zhang and Balasubramanian (ZB), who calculated potential energy surfaces (PESs) for interaction of several spin states of Pt^+ with H_2 at the complete active space self-consistent field (CASSCF) level.[33] Single point calculations on the stationary points were then conducted at a multireference single and double configuration interaction (MRSDCI) level. These calculations use a relativistic effective core potential on Pt that retains the ns and $(n-1)d$ orbitals in the valence space. In all of these calculations, the symmetry was restricted to C_{2v} and excited surfaces having the same symmetry as lower energy surfaces were not included in the work. (The energies given for these results in Table IV may need to be corrected for the Pt^+ spin–orbit asymptote, which would systematically decrease them by 0.418 eV. Such a correction is not applied to the results of ZB as this makes the agreement with experiment and the present calculations considerably worse.)

For PtH_2^+, our calculations find an inserted $^2A_1$ ground state with a BDE of 1.60 eV (Table IV), consistent with an experimental value of 1.52±0.12 eV determined recently.[46] The MRSDCI BDE of ZB, 1.20 eV, is somewhat weaker than this experimental value, and they also find a $Pt^+(H_2)$ adduct along the same $^2A_1$ surface (Table IV).[33] B3LYP calculations of the potential energy surface were conducted to locate this state, and are shown in Fig. 4. In contrast to the CASSCF calculations, we find no barrier preventing this adduct from spontaneously inserting to form the inserted ground state. The $^2A_2$, $^2B_1$, and $^2B_2$ surfaces shown are qualitatively consistent with the CASSCF surfaces of ZB but in all cases the large angle minima in the B3LYP calculations are lower in energy, more consistent with the energies calculated at the MRSDCI level (Table IV). ZB also calculate several quartet surfaces evolving from the excited state $Pt^+(^4F)$ asymptote, but in all cases, these are repulsive at long range and therefore do not interact with the doublet surfaces in regions that are important experimentally. Therefore, we did not include the quartet surfaces in our theoretical work.

Because of the C_{2v} symmetry restriction, the PESs in Fig. 4 and those of ZB cannot examine the PtH^+ + H dissociation asymptote. We anticipate that these products are formed from the PtH_2^+ intermediates with no barriers in excess of the endothermicity for the following reasons. Ground states of PtH^+ ($^3\Delta,^1\Sigma^+$) can interact with H (^2S) to form both low-spin doublet and high-spin quartet states of PtH_2^+. Formation of the low-spin doublet states involves covalent coupling of a nonbonding $PtH^+(^3\Delta)$ electron with H, such that the PESs should be strongly attractive, or donation of the electron on H into an empty orbital on $PtH^+(^1\Sigma^+)$, which should also lead to an attractive surface. To verify this hypothesis, we performed relaxed potential energy surface scans at the B3LYP/HW+/6-311+G(3p) level starting with the bound PtH_2^+ species and systematically lengthening one of the Pt–H bonds. We examined both a $^2A'$ surface, evolving from $PtH_2^+(^2A_1)$, and a $^2A''$ surface, evolving from $PtH_2^+(^2A_2,^2B_1)$. In the latter case only, we were forced to hold the other Pt–H bond length constant, which is reasonable as the bond lengths do not change appreciably from inserted PtH_2^+ to PtH^+, Table V. Without this constraint, the surface followed a path in which the H_2 molecule was removed from Pt^+. As shown in Fig. 5, both the $^2A'$ and $^2A''$ surfaces lead directly to PtH^+ + H products with no barriers in excess of the endothermicity. For the $^2A'$ surface, the asymptotic PtH^+ bond length corresponds to that for the $^3\Delta$ state; whereas because of the constraints on the geometry for the $^2A''$ surface, it is unclear whether the $^1\Sigma^+$ or $^3\Delta$ state of PtH^+ is actually formed.

Finally, we also considered a collinear reaction between Pt^+ and H_2. The qualitative rationale for this study is the

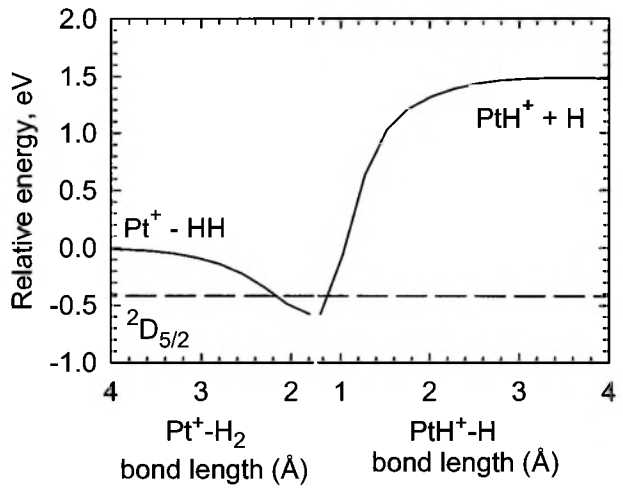

FIG. 6. B3LYP/HW+/6-311+G(3p) calculations of the potential energy surfaces for the interaction of $Pt^+(^2D)$ with H_2 in $C_{\infty v}$ symmetry as a function of the Pt^+-H_2 bond length (left side) and PtH^+-H bond length (right side) in angstroms. A dashed line indicates the experimental energy zero, corresponding to the $Pt^+(^2D_{5/2})$ ground state at -0.418 eV.

fact that $Pt^+(^2D)$ has a single unpaired electron, naively making it similar to $H(^2S)$ which is known to react with H_2 along a collinear $C_{\infty v}$ path, rather than a perpendicular C_{2v} path. Clearly, $Pt^+(^2D)$ is more complicated and electronically richer than $H(^2S)$, but the collinear pathway is also found to be a viable mechanism for reaction with H_2 as shown in Fig. 6. Initial approach of $Pt^+(^2D)$ to H_2 is attractive when the d_{z2} orbital (lying along the internuclear axis) is singly occupied. This surface forms a Pt^+-H-H adduct in which the Pt–H bond length is 1.794 Å and the H–H bond length is 0.773 Å, similar to that calculated for free H_2, 0.743 Å. This minimum lies 0.58 eV below the reactant asymptote and 0.16 eV below the experimental zero at $Pt^+(^2D_{5/2})+H_2$. From this adduct, lengthening the H–H bond leads cleanly to $PtH^+(^1\Sigma^+)+H$ products, as expected for a surface in which the electron hole starts in the d_{z2} orbital. For a collinear path to lead diabatically to $PtH^+(^3\Delta)+H$, the d_{z2} orbital would have to be doubly occupied, leading to a more repulsive interaction in the entrance channel (as verified theoretically). However, small deviations from exactly collinear paths could relieve such constraints, thereby permitting adiabatic formation of $PtH^+(^3\Delta)+H$.

VI. DISCUSSION

σ-bond activation by atomic metal ions can be understood using a simple donor–acceptor model. When an H_2 molecule approaches a transition metal ion, M^+, in a perpendicular direction (C_{2v} symmetry), the most efficient reaction occurs when M^+ accepts electrons from the $\sigma(H_2)$ bonding orbital into an empty ns or $(n-1)d\sigma$ orbital and donates a pair of $(n-1)d\pi$ electrons into the $\sigma^*(H_2)$ antibonding orbital. These interactions effectively weaken and lengthen the H_2 bond while simultaneously building electron density between the metal and H atoms. If the valence ns or $(n-1)d\sigma$ orbitals are occupied, then there is a more repulsive interaction between M^+ and H_2 that can be reduced if the H_2 approaches M^+ in a collinear geometry ($C_{\infty v}$ symmetry).

With this donor–acceptor model in mind, the qualitative behavior of the surfaces shown in Figs. 4 and 6 can be understood. For $Pt^+(^2D,5d^9)$, the $5d\sigma$ orbital can be singly occupied, such that a collinear reactant approach might be expected. Indeed, calculations indicate that this configuration has a favorable interaction with H_2 that leads directly to PtH^++H products (Fig. 6). However, the empty $6s$ orbital of $Pt^+(^2D,5d^9)$ allows a strong interaction in C_{2v} symmetry as well, which may be enhanced by $6s-5d\sigma$ hybridization. In explaining the qualitative behavior of the surfaces in Fig. 4, we define the orientation of the orbitals such that z lies along the C_{2v} symmetry axis and the three atoms lie in the $x-z$ plane. Then, the four surfaces shown, $^2A_1$, $^2A_2$, $^2B_1$, and $^2B_2$, involve singly occupied d_{z2}, d_{xy}, d_{yz}, and d_{xz} orbitals, respectively. The $^2A_1$ surface is most attractive because it has the electron hole in the orbital pointed at the doubly occupied $\sigma_g(H_2)$ orbital. The $^2B_2$ surface is attractive only at long range because, in contrast to the other surfaces, there is only one electron in the d_{xz} orbital which donates electron density into the empty antibonding $\sigma_u(H_2)$ orbital, thus helping to break the H_2 bond. A fifth surface, $^2A_1$, that also must evolve from the $Pt^+(^2D)+H_2$ asymptote has an electron hole in the d_{x2-y2} orbital such that it might be anticipated to behave most like the $^2A_2(d_{xy})$ surface.

Like Pt^+, the ^2D ground states of Ni^+ and Pd^+ have $(n-1)d^9$ configurations with empty ns and occupied $(n-1)d\sigma$ orbitals. The platinum system has about three times higher reactivity towards dihydrogen than the palladium system,[12] whereas the palladium system is about 1.5 times as reactive as the nickel system.[7,9] The larger reactivity for the platinum system is partly a consequence of the smaller endothermicity, 1.67 ± 0.05 eV vs 2.41 ± 0.04 eV for Pd^+ and 2.80 ± 0.08 eV for Ni^+. As described in detail by Ohanessian *et al.*,[26] this is largely a consequence of the lanthanide contraction and relativistic effects that allow efficient $6s-5d\sigma$ hybridization. Further comparison of the group 10 metal ions requires more information about the reaction mechanisms as revealed by the studies with HD.

Previous work on the first-row and second-row transition metal cations indicates that the product branching ratio in the reaction of M^+ with HD is very sensitive to the reaction mechanism.[9,12,13,19,20,49] Three categories of reactivity have been established for the first-row transition metal cations and depend on their electron configuration and spin state of metal ions. (1) If M^+ has an electron configuration with empty $4s$ and $3d\sigma$ orbitals, such as for a $3d^x$ configuration where $x<5$, the reaction is efficient and may proceed by an insertion mechanism. These processes are characterized by a product branching ratio in the HD system, $\sigma(MH^++D)/\sigma(MD^++H)$, that is near unity, consistent with statistical decomposition of a long-lived intermediate. (2) If either the $4s$ or $3d\sigma$ orbital is occupied and the M^+ state is low-spin, such as $3d^x(x>5)$ or low-spin coupled $4s^13d^{x-1}$ configurations, the reaction occurs efficiently via a direct mechanism. These processes are characterized by a product branching ratio in the HD system that favors MH^+ by a factor of 2–4, consistent with arguments concerning the conservation of angular

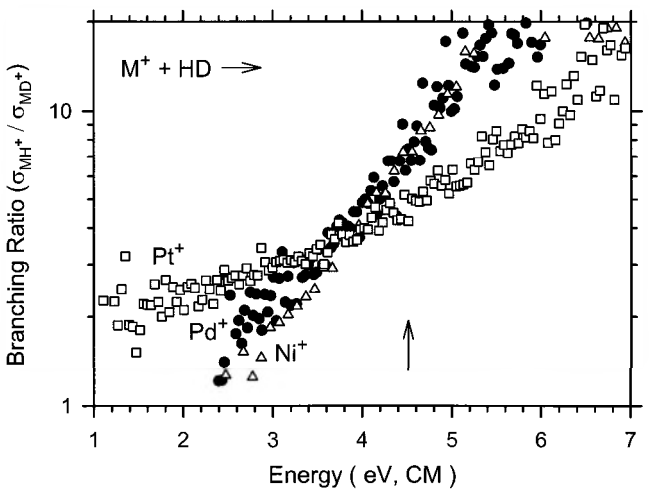

FIG. 7. Product branching ratios ($\sigma_{MH^+}/\sigma_{MD^+}$) for reactions of Ni^+ (open triangles), Pd^+ (solid circles), and Pt^+ (open squares) with HD as a function of kinetic energy in the center-of-mass frame. The arrow indicates D_0(H–D) at 4.51 eV.

momentum.[48,59,63–65] (3) If either the $4s$ or $3d\sigma$ orbital is occupied and the M^+ state is high-spin (the highest spin it can possibly have), such as high-spin coupled $4s^1 3d^{x-1}$ configurations, the reaction is inefficient and tends to react impulsively. These processes are characterized by a product branching ratio in the HD system that favors $MD^+ + H$ by a large factor and exhibits shifts in the thresholds for the H_2 and D_2 systems vs the HD system. Note that these rules are only appropriate for the diabatic reaction behavior, i.e., cases where the electron configuration of the metal ions remains essentially static throughout the course of the reaction.

In accordance with rule 2, Ni^+ and Pd^+ exhibit branching ratios associated with a direct mechanism in the reaction of M^+ with HD,[9,12] and it is therefore anticipated that Pt^+ might also react via a direct mechanism. A cursory comparison of the data for reactions of Ni^+, Pd^+, and Pt^+ reveals many similarities, suggesting that Pt^+ does follow the same mechanistic behavior. However, a closer scrutiny of the branching ratios in the HD systems, Fig. 7, shows differences among the three systems. Clearly, the Ni^+ and Pd^+ systems have very similar behavior, differing slightly at the lowest energies because the thresholds for reaction are somewhat different. In all three systems, the reactions favor formation of $MH^+ + D$ by factors near 2 at threshold and then rapidly increase, consistent with a largely direct reaction. However, the Pt^+ system does not increase nearly as rapidly as its lighter congeners, suggesting that its behavior is mediated by other effects. These other considerations are suggested by the calculated potential energy surfaces which indicate that the reaction could proceed via a long-lived stable PtH_2^+ intermediate, thereby leading to statistical behavior and a near one-to-one PtH^+/PtD^+ ratio. The combination of these direct and statistical pathways may provide the isotopic behavior observed. We speculate that the dynamics of the reaction is such that formation of $PtH^+ + H$ products is most efficient via direct pathways, but that the availability of stable dihydride intermediates on the global PES allows the reaction of Pt^+ to be more statistical than its lighter congeners, Fig. 7. Another possible mediating factor could be differences in the mechanisms associated with formation of $PtH^+(^1\Sigma^+)$ and $PtH^+(^3\Delta)$, but this cannot be ascertained from the present work.

VII. CONCLUSIONS

Ground state Pt^+ ions are highly reactive with dihydrogen over a wide range of kinetic energies, as compared with the first-row and second-row transition metal systems. Analysis of the kinetic energy dependence of the reaction cross sections provides the BDE of $Pt^+–H$, which is in agreement with *ab initio* calculations performed here and in the literature. The bond of the $PtH^+(^3\Delta)$ ground state is stronger than those of the other group 10 metal ions, Ni^+ and Pd^+, which is attributed to effective $6s–5d\sigma$ hybridization, a consequence of lanthanide contraction and relativistic effects.[26] The $^1\Sigma^+$ state of PtH^+ has a bond energy comparable to the $^3\Delta$ state, because it requires no promotion or loss of exchange energy. In this case, the bond is stronger than the first and second row congeners because the $5d$ orbital is better matched to bond to the H($1s$) than the $3d$ and $4d$ orbitals.[26]

In the Pt^+ system, calculations find that reactions with H_2 occur on surfaces of doublet spin without a barrier. The branching ratios observed in the $Pt^+ + HD$ reactions indicate that the ground state of Pt^+ reacts with dihydrogen largely via a direct mechanism. However, the mechanism exhibits differences from those of the first and second row congeners, Ni^+ and Pd^+. This can be rationalized using the theoretical results, which show that reaction at all angles of approach between the platinum ion and H_2 are reasonably favorable. Thus, the reactions of Pt^+ differ from those of the lighter congeners because more statistical pathways involving insertion intermediates are available.

ACKNOWLEDGMENTS

This work was supported by the National Science Foundation under Grant No. CHE-9877162 and CHE-0135517. X.-G.Z. thanks Dr. Rohana Liyanage for technical help with experiments.

[1] P. B. Armentrout and J. L. Beauchamp, Chem. Phys. **50**, 37 (1980).
[2] P. B. Armentrout and J. L. Beauchamp, J. Am. Chem. Soc. **103**, 784 (1981).
[3] P. B. Armentrout, L. F. Halle, and J. L. Beauchamp, J. Am. Chem. Soc. **103**, 962 (1981).
[4] P. B. Armentrout, L. F. Halle, and J. L. Beauchamp, J. Am. Chem. Soc. **103**, 6501 (1981).
[5] L. F. Halle, F. S. Klein, and Beauchamp, J. Am. Chem. Soc. **106**, 2543 (1984).
[6] M. A. Tolbert and J. L. Beauchamp, J. Am. Chem. Soc. **106**, 8117 (1984).
[7] J. L. Elkind and P. B. Armentrout, J. Phys. Chem. **90**, 6576 (1986).
[8] J. L. Elkind and P. B. Armentrout, Inorg. Chem. **25**, 1078 (1986).
[9] J. L. Elkind and P. B. Armentrout, J. Phys. Chem. **91**, 2037 (1987).
[10] M. L. Mandich, L. F. Halle, and J. L. Beauchamp, J. Am. Chem. Soc. **106**, 4403 (1984).
[11] J. L. Elkind, L. S. Sunderlin, and P. B. Armentrout, J. Phys. Chem. **93**, 3151 (1989).
[12] Y.-M. Chen, J. L. Elkind, and P. B. Armentrout, J. Phys. Chem. **99**, 10438 (1995).
[13] M. R. Sievers, Y.-M. Chen, and P. B. Armentrout, J. Phys. Chem. **100**, 54 (1996).

[14] P. B. Armentrout, R. V. Hodges, and J. L. Beauchamp, J. Chem. Phys. **66**, 4683 (1977).
[15] P. B. Armentrout, R. V. Hodges, and J. L. Beauchamp, J. Am. Chem. Soc. **99**, 3163 (1977).
[16] P. B. Armentrout and J. L. Beauchamp, Chem. Phys. **48**, 315 (1980).
[17] R. Georgiadis and P. B. Armentrout, J. Phys. Chem. **92**, 7060 (1988).
[18] N. F. Dalleska, K. C. Crellin, and P. B. Armentrout, J. Phys. Chem. **97**, 3123 (1993).
[19] P. B. Armentrout, ACS Symp. Ser. **428**, 18 (1990).
[20] P. B. Armentrout, Int. Rev. Phys. Chem. **9**, 115 (1990).
[21] R. H. Crabtree, *The Organometallic Chemistry of the Transition Metals*, 2nd ed. (Wiley, New York, 1994).
[22] G. A. Somorjai, *Introduction to Surface Chemistry and Catalysis* (Wiley, New York, 1994).
[23] P. B. Armentrout and B. L. Kickel, in *Organometallic Ion Chemistry*, edited by B. S. Freiser (Kluwer, Dordrecht, 1996), p. 1.
[24] P. B. Armentrout, in *Topics in Organometallic Chemistry*, edited by J. M. Brown and P. Hofmann (Springer-Verlag, Berlin, 1999), Vol. 4-I, p. 1.
[25] P. B. Armentrout, Int. J. Mass. Spectrom. **200**, 219 (2000).
[26] G. Ohanessian, M. J. Brusich, and W. A. Goddard, III, J. Am. Chem. Soc. **112**, 7179 (1990).
[27] K. Balasubramanian and D. Dai, J. Chem. Phys. **93**, 7243 (1990).
[28] K. K. Das and K. Balasubramanian, J. Chem. Phys. **94**, 3722 (1991).
[29] D. Dai and K. Balasubramanian, J. Chem. Phys. **95**, 4284 (1991).
[30] D. Dai and K. Balasubramanian, Chem. Phys. Lett. **185**, 165 (1991).
[31] D. G. Dai, W. Cheng, and K. Balasubramanian, J. Chem. Phys. **95**, 9094 (1991).
[32] K. Balasubramanian and Z. Ma, J. Phys. Chem. **95**, 9794 (1991).
[33] H. Zhang and K. Balasubramanian, J. Phys. Chem. **96**, 6981 (1992).
[34] S. K. Loh, D. A. Hales, L. Lian, and P. B. Armentrout, J. Chem. Phys. **90**, 5466 (1989).
[35] R. H. Schultz and P. B. Armentrout, Int. J. Mass Spectrom. Ion Processes **107**, 29 (1991).
[36] E. Teloy and D. Gerlich, Chem. Phys. **4**, 417 (1974).
[37] D. Gerlich, Adv. Chem. Phys. **82**, 1 (1992).
[38] K. M. Ervin and P. B. Armentrout, J. Chem. Phys. **83**, 166 (1985).
[39] P. J. Chantry, J. Chem. Phys. **55**, 2746 (1971).
[40] X.-G. Zhang and P. B. Armentrout (unpublished).
[41] B. L. Kickel and P. B. Armentrout, J. Am. Chem. Soc. **117**, 4057 (1995).
[42] D. E. Clemmer, Y.-M. Chen, F. A. Khan, and P. B. Armentrout, J. Phys. Chem. **98**, 6522 (1994).
[43] C. L. Haynes and P. B. Armentrout, Organometallics **13**, 3480 (1994).
[44] B. L. Kickel and P. B. Armentrout, J. Am. Chem. Soc. **117**, 764 (1995).
[45] C. E. Moore, *Atomic Energy Levels*, Natl. Stand. Ref. Data Ser. (U.S., Natl. Bur. Stand.) **III**, 35 (1971).
[46] X.-G. Zhang, R. Liyanage, and P. B. Armentrout, J. Am. Chem. Soc. **123**, 5563 (2001).
[47] W. J. Chesnavich and M. T. Bowers, J. Phys. Chem. **83**, 900 (1979).
[48] N. Aristov and P. B. Armentrout, J. Am. Chem. Soc. **108**, 1806 (1986).
[49] P. B. Armentrout, in *Advances in Gas Phase Metal Ion Chemistry*, edited by N. G. Adams and L. M. Babcock (JAI, Greenwich, 1992), Vol. 1, p. 83.
[50] F. Muntean and P. B. Armentrout, J. Chem. Phys. **115**, 1213 (2001).
[51] K. P. Huber and G. Herzberg, *Molecular Spectra and Molecular Structure* (Van Nostrand Reinhold, New York, 1979), Vol. IV.
[52] A. D. Becke, J. Chem. Phys. **98**, 5648 (1993).
[53] C. Lee, W. Yang, and R. G. Parr, Phys. Rev. B **37**, 785 (1988).
[54] M. J. Frisch, G. W. Trucks, H. B. Schlegel *et al.*, GAUSSIAN 98, Revision A.7, Gaussian, Inc., Pittsburgh, PA, 1998.
[55] P. J. Hay and W. R. Wadt, J. Chem. Phys. **82**, 299 (1985).
[56] M. Pavlov, M. R. A. Blomberg, Per E. M. Siegbahn, R. Wesendrup, C. Heinemann, and H. Schwarz, J. Phys. Chem. A **101**, 1567 (1997).
[57] J. B. Foresman and Æ. Frisch, *Exploring Chemistry with Electronic Structure Methods*, 2nd ed. (Gaussian Inc., Pittsburgh, 1996).
[58] X.-G. Zhang, C. Rue, S.-Y. Shin, and P. B. Armentrout, J. Chem. Phys. **116**, 5574 (2002), following paper.
[59] J. L. Elkind and P. B. Armentrout J. Phys. Chem. **89**, 5626 (1985).
[60] P. B. Armentrout, in *Gas Phase Inorganic Chemistry*, edited by D. H. Russell (Plenum, New York, 1989), p. 1.
[61] P. B. Armentrout, in *Selective Hydrocarbon Activation: Principles and Progress*, edited by J. A. Davies, P. L. Watson, A. Greenberg, and J. F. Liebman (VCH, New York, 1990), p. 467.
[62] M. E. Weber, J. L. Elkind, and P. B. Armentrout, J. Chem. Phys. **84**, 1521 (1986).
[63] L. S. Sunderlin, N. Aristov, and P. B. Armentrout, J. Am. Chem. Soc. **109**, 78 (1987).
[64] J. D. Burley, K. M. Ervin, and P. B. Armentrout, Int. J. Mass Spectrom. Ion Processes **80**, 153 (1987).
[65] P. B. Armentrout, ACS Symp. Ser. **502**, 194 (1992).